Table 2. Features of Laser for Medical Field

1.	The safety and the non-invasiveness are guaranteed by choosing non-injurious wavelengths.
2.	From the view point of mutual interaction between light and a living body, it is possible to analyze the properties of cells and tissues.
3.	It can be applied broadly when measuring the targets, because the beams can be transferred through the thin fiber.
4.	The advantages of easy portability are afforded by the downsized probes.
5.	It is capable to give a simple and fast diagnosis by developing a new software program for analyses.

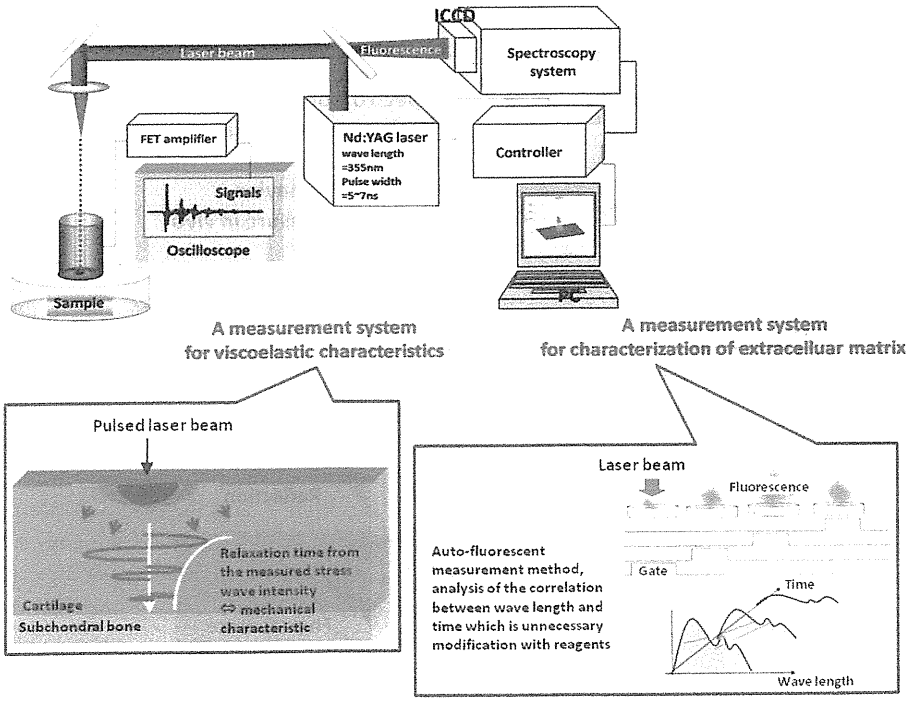

Figure 2. Simultaneous measurement system: photoacoustic measurement of viscoelastic characteristics and fluorescent measurement with time-resolved autofluorescence spectroscopy

EVALUATION OF MECHANICAL CHARACTERISTICS USING A PHOTOACOUSTIC METHOD

Tissue viscoelasticity affects the propagation and attenuation of the stress waves induced by pulsed laser irradiation [11]. The relaxation time of the stress wave, calculated as the time in which the amplitude of the stress wave decreases by a factor of 1/e, gives the intrinsic relaxation parameters (η/G) of the tissue, where η is the viscosity and G is the elasticity. We have proposed a basic principle whereby the mechanical characteristics of the tissue can be measured with photoacoustic parameters. In this measurement technique, the relaxation time of the stress that acts on a linear viscoelastic object (consisting of a spring and a dashpot) is related to the viscoelastic parameters of the object, and to the damping time of the stress waves that are generated by irradiation with a nanosecond pulse laser. The relaxation time is theoretically related to the viscous-to-elastic modulus rate [12]. The relaxation time (τ) is calculated using the Levenberg–Marquardt algorithm, a nonlinear least-squares method, as follows. When the stress wave intensity is attenuated only by its reflection at the boundaries and its relaxation during its transmission through viscoelastic materials, then the time course of the stress wave intensity is expressed by the following equation [2]:

$$I_\delta = I_0 \times R \times exp\ (-t_\delta / \tau)$$

where Io is the intensity of the stress wave at t = 0, R is the product of reflectivity (the product of the internal reflectivity at the interface at both ends of the sample), t_δ is the time after laser irradiation, and τ is the decay time of the stress wave and corresponds to the ratio of viscosity to elasticity.

Because the optimum wavelength of the laser beam was unknown at the beginning of this study, we used an optical parametric oscillator (Spectra-Physics K.K., Tokyo, Japan) and set the oscillation wavelength within the range of 250–355 nm, with collagen and protein as the optical chromophore, and it was thus possible to measure the photoacoustic signals at any wavelength within this range [11]. The shorter wavelengths within this wavelength range can magnify the absorption by living organs, so it is possible to increase the peak value of the initiated photoacoustic waves and to set the initiation depth of the photoacoustic wave at a shallower level. However, in practical terms, a small, portable, and inexpensive excitation light source is desirable, so we devised a system in which the third harmonic frequency of a Q switch Nd:YAG laser (wavelength 355 nm, pulse width 5–6 ns; Excel Technology K.K., Japan) was used [13,14]. We developed a probe in which the optical output was introduced via a quartz glass optical fiber (core diameter 400 nm; Thorlabs Japan Inc., Japan), and the poly(polyvinylidene fluoride) copolymer (P[VdF/TrFE]) of a piezoelectric polymer film (Nishiki Trading Co., Ltd., Japan) was used to detect the photoacoustic waves [14]. In this system, the laser irradiation side and the measuring side were originally opposite, so it was only possible to evaluate permeable objects in vitro. However, with repeated trial and error, we developed an integrated optical fiber reflective probe that allowed measurements to be made in vivo, specifically during arthroscopy, by situating the probe at the center and placing the sensors peripherally around it in a circle (Figure 3).

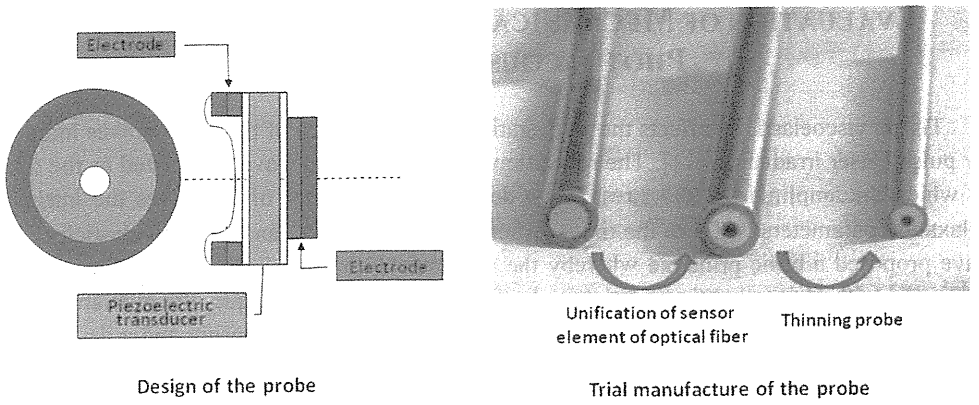

Figure 3. Development of the probe

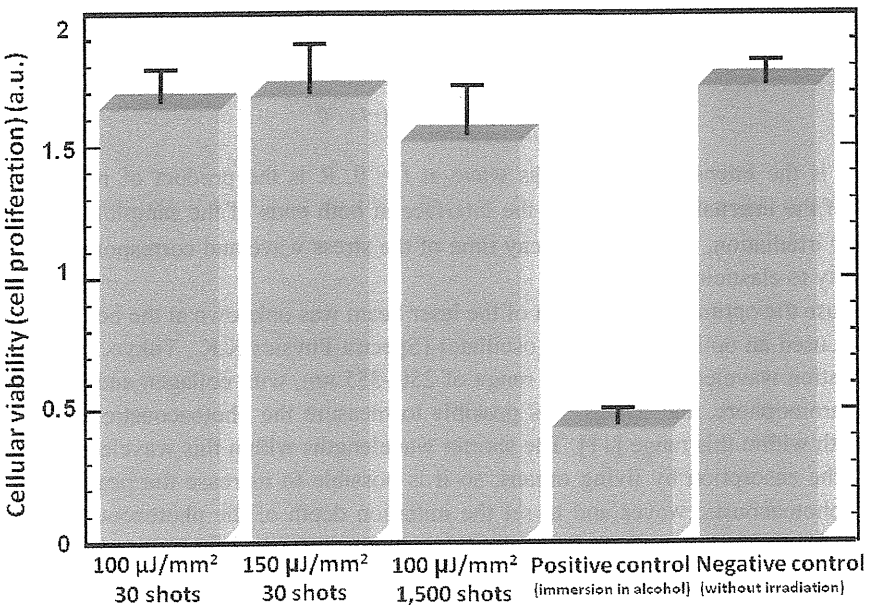

Figure 4. Effect of laser irradiation (energy per mm^2) on cell viability (cell proliferation)

SAFETY TEST

To assess the safety of the photoacoustic measurement method, we used a cell proliferative activity test in cultivated domestic rabbit chondrocytes and examined the effects on the chondrocytes of laser beam irradiation that induced photoacoustic signals. Because the irradiation conditions of the laser were based on the third harmonic generation of a Q switch

Nd:YAG laser with a wavelength of 355 nm, the following five groups were established and examined: (1) a group treated under clinically used radiation conditions (100 $\mu J/mm^2$, 30 shots); (2) a group treated under conditions in which the pulse energy was 1.5 times greater than that used clinically (150 $\mu J/mm^2$, 30 shots); (3) a group treated under conditions in which the number of pulse shots was 50 times higher than the number used clinically (150 $\mu J/mm^2$, 1,500 shots); (4) a positive control group to which 70% ethanol was added to kill the cells completely; and (5) a negative control with no laser irradiation. It should be noted that the pulse energy used to treat group (2) was the maximum output of this device. A WST-8 assay (Dojindo Laboratories, Japan) was used for the cell proliferative activity test. We applied the abovementioned conditions to cultivated cells sown in a 96-well plate and cultured at 37 °C under 5% CO_2, with all measurements made after 1 h. We confirmed that there were no significant differences between any laser-irradiated group and the nonirradiated group, so laser irradiation had no effect on cell proliferative activity (Figure 4) [14].

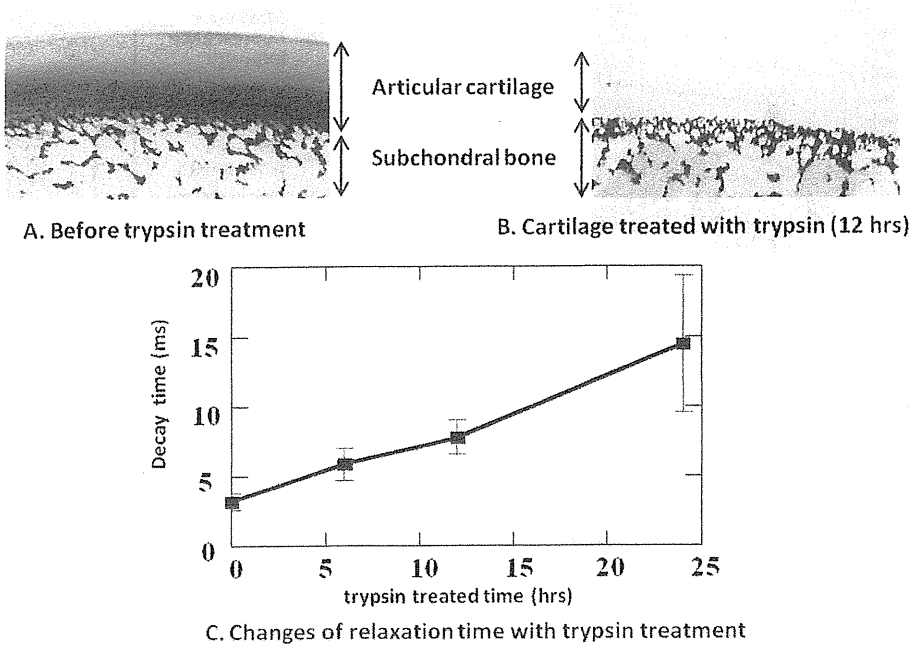

Figure 5. The photoacoustic evaluation of characteristic viscoelastic changes with cartilage degeneration

Evaluation of Degenerated Cartilage

To produce experimentally degenerated cartilage, we created cartilage with different degrees of degradation by extracting osteochondral plugs, with a diameter of 12 mm, from swine patellar cartilage and processing them with trypsin (trypsin–1 × EDTA; Gibco,

Invitrogen Corp., Carlsbad, Canada) to cause an outflow of proteoglycan, reflecting the changes in the mechanical characteristics of the tissue in vivo. The trypsin concentration was 1 mg/mL and it was applied for up to 24 h. We assessed the degenerated cartilage using the photoacoustic measurement method. After the measurements had been made, the samples were fixed in 10% formalin solution for histological study. The samples were sectioned to 4 μm thick slices for microscopic observation and stained with toluidine blue. Figure 5 shows the positive correlation between the decay time and the trypsinization time [14]. Specifically, the decay time increased as the trypsinization time increased. In other words, the viscosity increased and the elasticity decreased. Histologically, the stainability of the tissue with toluidine blue also decreased with trypsinization and the loss of proteoglycans, suggesting that it is possible to monitor the course of the tissue changes involved in cartilage degeneration using the photoacoustic measurement method.

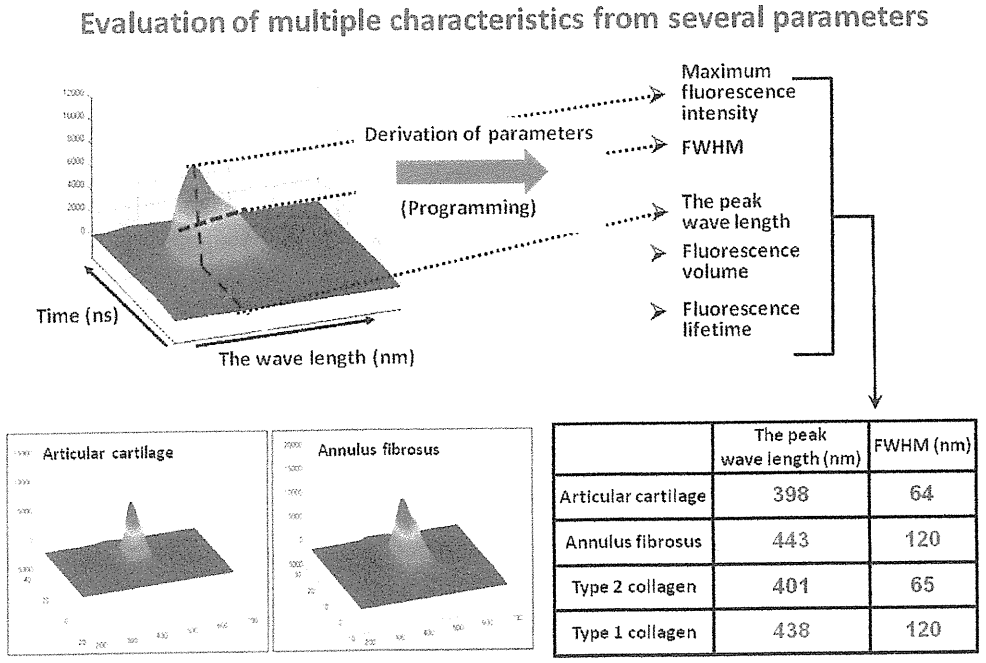

	The peak wave length (nm)	FWHM (nm)
Articular cartilage	398	64
Annulus fibrosus	443	120
Type 2 collagen	401	65
Type 1 collagen	438	120

Figure 6. Analyses with time-resolved autofluorescence spectroscopy

Property Evaluation Using Time-Resolved Autofluorescence Spectroscopy

For time-resolved autofluorescence spectroscopy, we used the third harmonic generation of the Q switch Nd:YAG laser for the excitation light introduced via an optical fiber, in a manner similar to that used in the photoacoustic measurement method. We used a CCD

sensor with an image intensifier as the photodetector, while controlling the spectroscopic system that could be measured by a nanosecond order gate with a four-channel digital pulse generator. The fluorescence peak intensity, half bandwidth, peak wavelength, fluorescence volume, and fluorescence life were calculated as the measurement parameters. The articular cartilage of Japanese white domestic rabbits, the outer layer of the annulus fibrosus, and commercially available type I and type II collagen (powder; Ieda Chemical Co., Ltd., Japan) were used as the target samples. The articular cartilage exhibited a spectrum close to that of type II collagen, and the peak wavelengths and half bandwidths were also similar. Conversely, the outer layer of the annulus fibrosus exhibited a spectrum close to that of type I collagen, and the peak wavelengths and half bandwidths were also similar (Figure 6) [2,12]. This indicates that it is possible to measure the collagen composition of tissue, because collagen is an autofluorescent substance used in vivo in a noncontact manner. This is significant because the content ratio of type I to type II collagen is especially important in diagnosing the degree of cartilage degradation[16].

APPLICATION IN THE MEDICAL FIELD

Many elderly people who suffer from lifestyle-related diseases are also affected by osteoarthritis and are often unable to perform exercises that would normally be within their physical capacity because of joint pain and a limited range of motion. This is particularly serious in patients with diabetes, hyperlipidemia, or obesity, and their disease may be exacerbated because osteoarthritis reduces their ability to exercise, even when exercise therapy is available. In osteoarthritis, evaluating the prognosis of conservative therapy or the treatment effects after surgery often depends on the patient's subjective symptoms, so the pathological condition is not accurately understood. Surgical treatments, such as artificial joint replacement, are currently performed on patients in the terminal phase, whereas patients in the initial to middle phases are treated conservatively, often without any clear aims.

This study has demonstrated that it is possible to evaluate the mechanical characteristics and properties of articular cartilage simultaneously during arthroscopy using a noninvasive intense pulsed laser. We are now developing a device for this application by trial and error. If such a device is developed, an accurate measurement of the mechanical characteristics of the original function of the articular cartilage and the associated tissue properties will be possible during arthroscopy, and anyone could make such a quantitative functional evaluation. Therefore, it will be possible to accurately understand the pathological features of osteoarthritis and to carefully plan and undertake treatments. This technology could also quantitatively measure and evaluate mechanical characteristics and tissue properties simultaneously, to assess treatment effects, such as those of a variety of drugs, in addition to the conventional evaluation of clinical symptoms such as pain or inflammation around the joints. We believe that this methodology will be useful in the objective evaluation of articular cartilage in the clinical trials of new drugs, etc. This diagnostic system is a methodology used during arthroscopy, so it cannot be a completely noninvasive evaluation [15]. However, if quantitative data are collected during arthroscopy treatments, it will be possible to predict the effects of a variety of conservative therapies, based on the severity of cartilage degeneration. Therefore, it will be possible to carefully plan and undertake treatments on an individual

patient basis. Accordingly, we are certain that the development of this technology and practical diagnostic devices will improve the patients' activities of daily living and quality of life, and thus contribute to a healthy life expectancy.

CONCLUSION

1. A photoacoustic measurement method using a noninvasive nanosecond-pulsed laser allowed the evaluation of the mechanical characteristics of cartilage, and time-resolved autofluorescence spectroscopy allowed the evaluation of tissue properties for analysis.
2. This measurement system, based on the interactions between optics and living organs, is an evaluation methodology suitable for making diagnoses during arthroscopy. It allows the quantitative and multidirectional evaluation of the original function of the cartilage based on a variety of parameters.

ACKNOWLEDGEMENTS

This work was supported by the Takeda Science Foundation, the General Insurance Association of Japan, Mitsui Sumitomo Insurance Welfare Foundation, a High-Tech Research Center Project for Private Universities, a Grant-in-Aid for Scientific Research, a Grant of the New Energy and Industrial Technology Development Organization, and the Health Labour Science Research Grant.

REFERENCES

[1] Yoshimura, N; Muraki, S; Oka, T; Kawaguchi, H & Nakamura, K. (2007). The 51st Annual General Assembly and Scientific Meeting of the Japan College of Rheumatology, *Program 265*.

[2] Ishihara, M; Sato, M; Kaneshiro, N; Mitani, G; Nagai, T; Kutsuna, T & Mochida, J. (2007). Usefulness and limitation of measurement methods for evaluation of tissue-engineered cartilage function and characterization using nanosecond pulsed laser. *Proceedings of SPIE 6439*: 643909.

[3] Ishihara, M; Sato, M; Kutsuna, T; Ishihara, M; Mochida, J & Kikuchi, M. (2008). Modification of measurement methods for evaluation of tissue-engineered cartilage function and biochemical properties using nanosecond pulsed laser. *Proceedings of SPIE 6858*: 685805.

[4] Ishihara, M; Sato, M; Ishihara, M; Mochida, J & Kikuchi, M. (2006). Multifunctional evaluation of tissue engineered cartilage using nano-pulsed light for validation of regenerative medicine. In: Kim SI and Suh TS, editors. *IFMBE Proceedings, World Congress on Medical Physics and Biomedical Engineering 14*; COEX Seoul, Korea. Springer: Berlin Heidelberg. p. 3187–9.

[5] Ishihara, M; Sato, M; Kaneshiro, N; Mitani, G; Mochida, J & Kikuchi, M. (2006).

Development of a noninvasive multifunctional measurement method using nanosecond pulsed laser for evaluation of regenerative medicine for articular cartilage. *Proceedings of SPIE 6084*: 60840V.

[6] Ishihara, M; Sato, M; Sato, S; Kikuchi, T; Mochida, J & Kikuchi, M. (2005). Usefulness of photoacoustic measurements for evaluation of biomechanical properties of tissue-engineered cartilage. *Tissue Eng.11*:1234–43.

[7] Ishihara, M; Sato, M; Sato, S; Kikuchi, T; Mitani, G; Kaneshiro, N; Kikuchi, M & Mochida, J. (2005). Usefulness of the photoacoustic measurement method for monitoring the regenerative process of full-thickness defects in articular cartilage using tissue-engineering technology. Progress in biomedical optics and imaging. *Proceedings of SPIE 5695*: 288–91.

[8] Ishihara, M; Sato, M; Mochida, J & Kikuchi, M. (2007). In: Akaike T (editor). *Regeneration Medicine 4*, Bioengineering for Regeneration Medicine. Corona Publishing Co., Ltd; p. 147–67.

[9] Ishihara, M; Sato, M; Mochida, J & Kikuchi, M. (2007). Noninvasive measurement for the evaluation and validation of regeneration medicine. *J. Biosci. Biotechnol. 85*:438–41.

[10] Ishihara, M; Sato, M; Mitani, G; Mochida, J & Kikuchi, M. (2007). Monitoring of extracellular matrix formation using nanosecond pulsed laser. *Journal of Institute of Electrical Engineers of Japan 127-C*: 2166—2170.

[11] Ishihara, M; Sato, M; Sato, S; Kikuchi, T; Fujikawa, K; Kikuchi, M. (2003). Viscoelastic characterization of biological tissue by photoacoustic measurement. *Jpn J. Appl. Phys.;42*:556–8.

[12] Han, C & Barnett, B. (1973). Measurement of the rheological properties. In: Gabelnick HL and Litt M, editors. *Rheology of Biological Systems*. Illinois: Charles C. Thomas Publisher, Ltd; p. 195–217.

[13] Ishihara, M; Sato, M; Kaneshiro, N; Mitani, G; Sato, S; Mochida, J & Kikuchi, M. (2005). Development of a photoacoustic measurement method for the evaluation of regenerative medicine and tissue engineering for articular cartilage. *J. Jpn Soc. Laser Surg. Med;26*:53–9.

[14] Ishihara, M; Sato, M; Kaneshiro, N; Mitani, G; Sato, S; Mochida, J & Kikuchi, M. (2006). Development of a diagnostic system for osteoarthritis using a photoacoustic measurement method. *Lasers Surg. Med., 38*:249–55.

[15] Sato, M; Ishihara, M; Furukawa, K; Kaneshiro, N; Nagai, T; Mitani, G; Ota, N; Kokubo M; Kikuchi, M & Mochida, J. (2008). Recent technological advancements related to articular cartilage regeneration. *Med. Biol. Eng. Comput.;46:*735–43.

[16] Kutsuna, T; Sato, M; Ishihara, M; Furukawa, K; Nagai, T; Kikuchi, M; Ushida, T & Mochida, J. (2009). Noninvasive Evaluation of Tissue Engineered Cartilage with Time-Resolved Laser-Induced Fluorescence Spectroscopy. *Tissue Eng. Part C Methods.* Jul 10. [Epub ahead of print]

PRIMARY IMMUNE SYSTEM RESPONDERS TO *NUCLEUS PULPOSUS* CELLS: EVIDENCE FOR IMMUNE RESPONSE IN DISC HERNIATION

Kunihiko Murai[1]*, Daisuke Sakai[2, 3], Yoshihiko Nakamura[3], Tomoko Nakai[3], Takashi Igarashi[1], Norimasa Seo[1], Takashi Murakami[4], Eiji Kobayashi[4], and Joji Mochida[2, 3]

[1]Department of Anesthesiology and Intensive Care Medicine, Jichi Medical University, 3311-1 Yakushiji, Shimotsuke, Tochigi, 329-0498, Japan
[2]Department of Orthopaedic Surgery, Surgical Science, Tokai University School of Medicine, 143 Shimokasuya, Isehara, Kanagawa, 259-1193, Japan
[3]Research Center for Regenerative Medicine, Tokai University School of Medicine, 143 Shimokasuya, Isehara, Kanagawa, 259-1193, Japan
[4]Division of Organ Replacement Research, Center for Molecular Medicine, Jichi Medical University, 3311-1 Yakushiji, Shimotsuke, Tochigi, 329-0498 Japan

Abstract

Although intervertebral disc herniation and associated sciatica is a common disease, its molecular pathogenesis is not well understood. Immune responses are thought to be involved. This study provides direct evidence that even non-degenerated *nucleus pulposus* (NP) cells elicit immune responses. An *in vitro* colony forming inhibition assay demonstrated the suppressive effects of autologous spleen cells on NP cells and an *in vitro* cytotoxicity assay showed the positive cytotoxic effects of natural killer (NK) cells and macrophages on NP cells. Non-degenerated rat NP tissues transplanted into wild type rats and immune-deficient mice demonstrated a significantly higher NP cell survival rate in immune-deficient mice. Immuno-histochemical staining showed the presence of macrophages and NK cells in the transplanted NP tissues. These results suggest that even non-degenerated autologous NP cells are recognized by macrophages and NK cells, which may have an immunological function in the early phase of disc herniation. These findings contribute to understanding resorption and the inflammatory reaction to disc herniation.

Keywords: *Nucleus pulposus*, immune response, macrophage, natural killer cell, intervertebral disc, autoimmunity.

*Address for correspondence:
Kunihiko Murai
Department of Anesthesiology and Intensive Care Medicine,
Jichi Medical University,
3311-1 Yakushiji, Shimotsuke, Tochigi, 329-0498, Japan
Telephone Number: +81 285 58 7383
FAX Number: +81 285 44 4108
E-mail: murai.mane@jichi.ac.jp

Introduction

Resorption of herniated *nucleus pulposus* (NP) is a clinically demonstrated phenomenon during intervertebral disc herniation. In understanding the undefined pathogenesis of intervertbral disc herniation and sciatica, clarifying the molecular events that occur in resorption of NP is important. Nachemson (1969) reported decreased pH levels within and around a herniated lumbar disc and speculated that sciatica was caused by an inflammatory reaction surrounding the nerve root. Subsequently, various inflammatory chemical factors secreted from herniated NP, including tumor necrosis factor (TNF)-α (Weiler *et al.*, 2005; Le Maitre *et al., 2007*), interleukin (IL)-1β (Le Maitre *et al., 2007*) and nitric oxide (NO) (Katsuno *et al.*, 2008), have been implicated as causes of sciatica (McCarron *et al*, 1987; Geiss *et al.*, 2007). Further, the production of matrix metalloproteinases (MMPs) has been implicated in the resorption of the herniated NP (Doita *et al.*, 2001).

Bobechko and Hirsh (1965) and Gertzbein *et al.* (1975) reported that herniated NP tissue is recognized as a foreign antigen that induces an autoimmune response producing inflammation. Later, immunohistochemical (IHC) analyses of human herniated discs revealed the presence of infiltrated T cells (Park *et al.*, 2001), macrophages (Park *et al.*, 2001; Virri *et al.*, 2001), and antigen-antibody complexes in the NP (Satoh *et al.*, 1999). An *in vitro* co-culture model of macrophages and NP cells also showed the infiltration of macrophages and a decreased wet weight of the NP (Haro *et al.*, 2000). The expression of IL-6, -8, -12, and interferon (IFN)-γ suggests Th1 lymphocyte activation (Kang *et al.*, 1996; Burke *et al.*, 2002; Park *et al.*, 2002). Geiss *et al.* placed autologous porcine NP in subcutaneous titanium chambers and observed the infiltration of activated T and B cells (Geiss *et al.*, 2007), including IL-4-producing Th2 cells and γδ T cells (Geiss *et al.*, 2008). These results indicate both innate and acquired immune responses to the NP. Other studies (Park *et al.*, 2001; Jones *et al.*, 2008), however, have reported that NP cells undergo apoptosis and are phagocytised by macrophages without an immune response. Ikeda *et al.* (1996) investigated infiltrated cells consisting of macrophages and a small number of T cells, and proposed that extruded or sequestrated disc material

has the potential to be absorbed by phagocytes. It remains unclear from these reports whether immune responses are truly involved in disc herniation, and if so, which immune cells initiate the immune response.

In order to investigate whether an immune response is involved in disc herniation, fundamental research on NP cells and the immune system is required. The purpose of this study is to clarify the immune response to autologous NP cells and to identify the specific immune cells that initiate an immune response by using *in vivo* and *in vitro* rat models to assess the survival of NP cells exposed to immune system cells.

Materials and Methods

In vitro studies

Preparation of rat-tail NP cells. Male Sprague-Dawley (SD) rats (Nihon Charles River Co., Kanagawa, Japan) aged 10-12 weeks, were used for the colony forming inhibition assay (CFI), and male Lewis rats (Nihon Charles River) aged 10-12 weeks were used for the cytotoxicity assay. Following sacrifice, NP tissues were dissected from the whole tail and digested in 0.05% trypsin-ethylene diamine tetraacetic acid (EDTA; Gibco, Grand Island, NY, USA) for 15 minutes. The digestate was washed, passed through a 100 μm mesh cell strainer, the NP cells were collected by mild centrifugation (500Gx4min). These experiments were approved by the Animal Research Committee of Tokai University (071095) and conducted according to the guidelines for animal experiments.

Preparation of spleen cells. Autologous spleen cells were used as effector cells for the CFI assay and isogenous spleen cells were used for the cytotoxicity assay. Briefly, the spleens were removed, mashed and passed through a 100 μm mesh cell strainer. Red blood cells were haemolysed using 0.8% NH_3Cl. The spleen cells were collected by mild centrifugation (500Gx4min). The spleen cells (10^7cells/ml) were then incubated in RPMI-1640 medium (Invitrogen, Grand Island, NY, USA) with 15% foetal bovine serum (FBS, Qualified FBS, Invitrogen) at 37°C for five hours with IL-2 (60 IU/ml; Imunase, Shionogi, Osaka, Japan).

Purification of T cells, natural killer (NK) cells and macrophages. For cytotoxicity assays, more than 10^8 of the spleen cells isolated from a Lewis rat were suspended in fluorescence-activated cell sorting (FACS) buffer (Facs Flow, Becton Dickinson (BD) Pharmingen, Tokyo, Japan) and incubated for 30 minutes at 4°C with saturating amounts of the following antibodies: CD3 (#550353, PE mouse anti-rat CD3, BD), CD4 (#550057 Pharmingen, APC mouse anti-rat CD4, BD), CD8 (#558824, Per CP mouse anti-rat CD8a, BD), CD161 (#550978, biotin mouse anti-rat CD161, BD). The labelled spleen cells were then separated into NK cells (CD161+), CD4+T cells (CD3+CD4+), CD8+T cells (CD3+CD8+), and macrophages (remaining CD3-) using a FACS Vantage (BD).

CFI assay. For the CFI assay, the suppressive effect of immune cells (effector cells) on colony formation by autologous NP cells (target cells) was assessed by a previously described method (Spitzer *et al.*, 1980). The NP cells isolated from SD rats (N=4) were immediately utilized for the assay procedures. NP cells ($6x10^3$) and autologous spleen cells were seeded for each E:T ratio of 0:1, 25:1, 50:1 and 100:1 in 6ml of 0.9% methylcellulose formation (MethoCult H4230 Stemcell Technologies, Vancouver, Canada) in a single tube, mixed completely, then we dispensed it by 1ml in 35mm dishes (n=4 for each E:T ratio). The dishes were incubated at 37°C in 5% CO_2 and full humidity for 14 days without medium replacement, after which the number of NP colonies was scored at least twice for each dish using a tally board on the bottom of the dishes.

Cytotoxicity assay. For the cytotoxicity assay, NP cells from Lewis rats (N=2) were monolayer cultured in RPMI-1640 medium with 15% FBS for 10 days. The cells were labeled using calcein-AM (Dojin Chemical Institute, Kumamoto, Japan) for 60 minutes at 37°C without serum, washed, and seeded into 96-well V-bottomed plates (#4914, Matrix Technologies, Hudson, NH, USA) at $1x10^4$ cells/ well. Suspensions of purified isogenous NK cells, CD4+ T cells, CD8+ T cells, or macrophage cells were then added to wells at E:T cell ratios of 0:1, 25:1, 50:1 and 100:1 in a final volume of 200 μL/well in RPMI-1640 medium without serum (n = 4 for each ratio). The plate was centrifuged, then incubated in humidified air for eight hours at 37°C. After incubation, the plates were centrifuged and 100 mL of supernatant from each well was moved to another 96 well flat-bottomed plate in the same pattern, and was measured using a fluorescent plate reader (λ_{ex}=485 nm, λ_{em}=520 nm, Beckman Coulter, Brea, CA, USA). Cytotoxic activity was determined according to a modification of the ^{3}H-uridine labelling method described by Wang *et al.* (1993). Cytotoxicity was calculated as:

$$\%\text{cytotoxicity} = \frac{\text{experimental release} - \text{spontaneous release}}{\text{total release} - \text{spontaneous release}} \times 100 \quad (1)$$

Total release was obtained by detergent solubilisation in the presence of 1% Triton X-100 (GE Healthcare Japan, Tokyo, Japan). Spontaneous release means the fluorescence release of the pure NP cell groups. Fibroblastic cells from the *anulus fibrosus* was also analyzed as negative control.

In vivo study

For *in vivo* studies, intact rat NP tissues were transplanted with PBS into immunodeficient mice and wild type rats. The survival rate of the NP cells in the transplanted tissue was measured using the bioluminescence imaging (BLI) method described below to estimate the influence of immunity on NP cell survival. IHC staining was done on the NP tissues from the rat model to detect attracted immune cells, which would indicate the initiation of an immune response.

Transplantation of NP for the BLI study

For the BLI analysis, four male Lewis rats 10-12 weeks of

age were used as recipients of NP tissues for the Lewis to Lewis (Lew-Lew) group and four male 10-12-week-old NOD/Shi-*scid* mice (Nihon Charles River) served as recipients of NP tissues for the Lewis to NOD (Lew-NOD) group. Transgenic (Tg) male Lewis rats (8-10 weeks of age) whose tissues express luciferase produced by repeated crossing of Tg rats and confirmed in the *Organ Replacement Research Department in Jichi Medical University* were used as NP tissue donors. 100 μg of NP tissues were injected with 100 μL of PBS under the abdominal skin of recipients under general anaesthesia using 2-3% isoflurane. One donor was used for each recipient. The BLI study was conducted using a IVIS system (Xenogen Corp., Hopkinton, MA, USA) with LivingImaging acquisition and analysis software. Briefly, animals were anesthetized with isoflurane and given 125 mg/kg D-luciferin substrate (Biosynth AG, Staad, Switzerland). The animals were then placed in a light-tight chamber for imaging with a CCD camera. The photon counts from the peak luciferase activity were recorded. Luciferase activity was measured as photons emitted/second. Imaging studies were performed immediately after transplantation and at day 7, day 14 and day 21.

IHC staining

For IHC staining, male Lewis rats (n=6) were newly used as recipients of NP tissues. The transplantation procedure was the same as for the Lew-Lew group described above and one donor was used for each recipient (n=6). Two recipients were sacrificed at 5, 10, and 40 days after transplantation. In addition, two NOD mouse in BLI study was sacrificed at 26 days after transplantation. After fixation with 10% formalin for three days, a paraffin block was made though an alcohol-xylene-paraffin graded series. Five-micron thick paraffin sections were cut sagittally from the epidermis to the peritoneal membrane across the transplantation site, deparaffinized 5-μm sections first were rehydrated through xylene and graded alcohol series. For double-staining immunofluorescence, tissue slides were incubated overnight at 4°C with a primary monoclonal antibody to keratan sulphate (KS) (#270427-1, mouse anti-KS, Associates of Cape Cod, Falmouth, MA, USA), diluted 1:100 in PBS with 1% BSA, followed by incubation in darkness at room temperature for three hours with Alexa Fluor 488-conjugated anti-mouse IgG diluted 1:200. After washing with PBS, the slides were incubated overnight at 4°C in darkness with diluted (1:100) primary antibodies for rat T cells (#550353, PE mouse anti-rat CD3, BD), macrophages (#sc-9139, rabbit anti-rat CD68, Santa Cruz Biotechnology, CA, USA), or NK cells (#550978, Biotin mouse anti-rat CD161, BD). After washing with PBS, the slides with CD68 were incubated for 60 minutes in room temperature with anti-rabbit goat Alexa 594 antibody (Invitrogen); slides with CD161 staining were incubated for one hour with streptavidin-Alexa 594 (Invitrogen). All slides were then covered with Vectashield mounting medium with DAPI (H-1500, Vector Laboratories, Burlingame, CA, USA). Sample sections of day 5, day 10 and day 40 were also stained with HE and Safranin-O.

Data Analysis

All data are given as the mean ± standard deviation (SD). The statistics were processed by Excel Stat 2006 (SSRI, Tokyo, Japan). Two-factor analysis of variance (ANOVA) was employed to analyze the *in vitro and in vivo results*. The Mann-Whitney U-test was used to compare the results of the two groups in CFI assay. When significant differences were revealed by the ANOVA, *post hoc* comparisons were done. Statistical significance was defined as $p < 0.05$.

Results

***In vitro* study**

CFI assay. Spleen cells from SD rats were used as effector cells for autologous tail NP target cells. Colony formation assays showed two types of colonies that were identified as CFU-A (adherent) and CFU-NA (non-adherent) when counting colonies. Without effector cells (E:T cell ratio of 0:1), NP cells ($1x10^3$) formed CFU-NA colonies ranging in numbers from 82-118 (94.8±18.1) and CFU-A colonies ranging from 39-60 (48.3±9.6). When effector cells were added, NP cells ($1x10^3$) with an E:T cell ratio of 25:1 yielded CFU-NA colonies ranging from 26-31 (29.0±2.2) and CFU-A colonies ranging from 22-38 (28.3±6.8), an E:T cell ratio of 50:1 resulted in CFU-NA colonies ranging from 19-26 (22.8±3.0) and CFU-A colonies ranging from 19-34 (26.8±6.6) and an E:T cell ratio of 100:1 produced CFU-NA colonies ranging from 19-25 (21.0±2.8) and CFU-A colonies ranging from 18-27 (21.0±4.2). The suppressive effect of spleen cells was apparent (Fig. 1A). CFU-NA colonies were affected stronger than CFU-A colonies (Table 1). Microscopic examinations of CFU-NA

Table 1 Percentage of the number of colonies to the control (E:T cell ratio = 0:1)

E:T cell ratio	0:1	25:1	50:1	100:1
CFU-NA (%)	100	30.6±2.3	24.0±3.2	22.2±3.0
CFU-A (%)	100	58.5±14.2	55.4±13.7	43.5±8.8
p-value		p=0.021	p=0.021	p=0.019

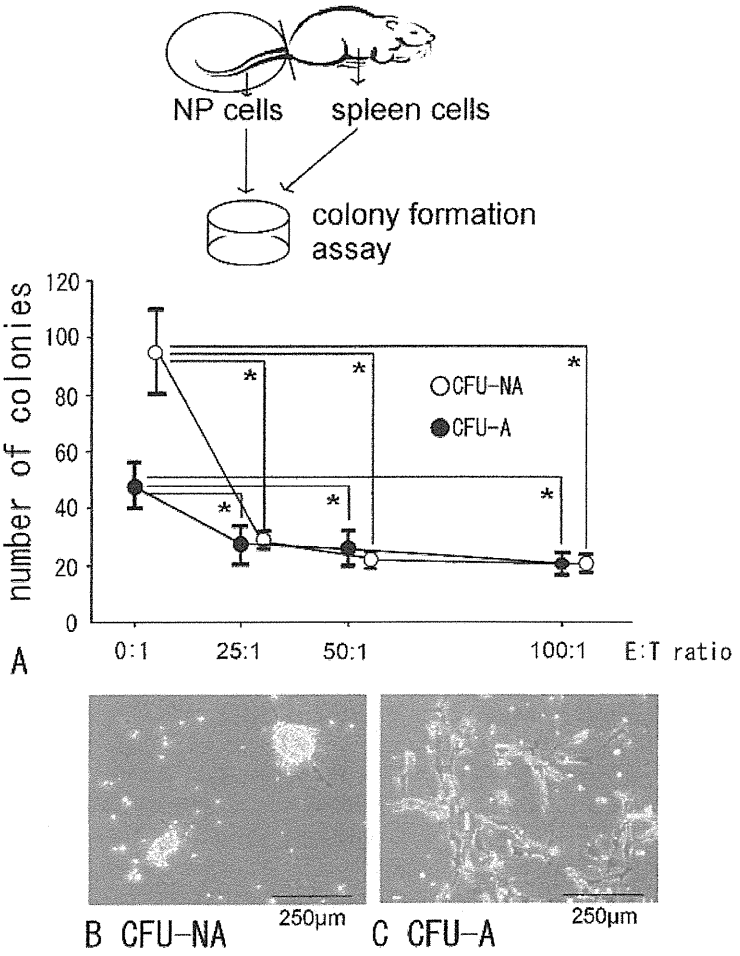

Fig. 1. (A) Results of CFI assay *in vitro*. Numbers of CFU-NA (open circle) and CFU-A (closed circle) colonies in the E: T ratio of 0:1, 25:1, 50:1 and 100:1 were counted at day 14. Colony formation of NP cells was suppressed by the addition of autologous spleen cells in both groups ($*p < 0.05$ compared with that in the E:T ratio of 0:1). (B) Attraction of spleen cells to CFU-NA. (C) Attraction of spleen cells to CFU-A. The larger number of spleen cells attracted to CFU-NA than to CFU-A supports the result in our current study that CFU-NA is more sensitive to autologous spleen cells.

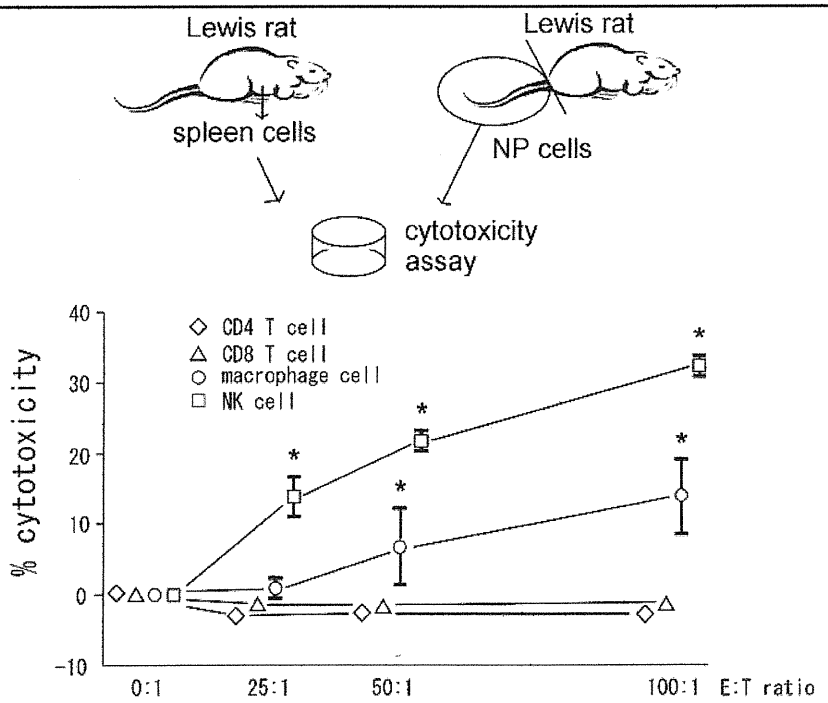

Fig. 2. Results of cytotoxicity assay *in vitro*. Cytotoxicity was calculated as follows,

$$\%\text{cytotoxicity} = \frac{\text{experimental release} - \text{spontaneous release}}{\text{total release} - \text{spontaneous release}} \times 100$$

0%=no cytotoxicity, 100%=maximum cytotoxicity as strong as detergent agent.
Cytotoxicity caused by NK cells and macrophages was suggested as a result of 8 hrs coculture ($*p < 0.05$ compared with that in the E:T ratio of 0:1).

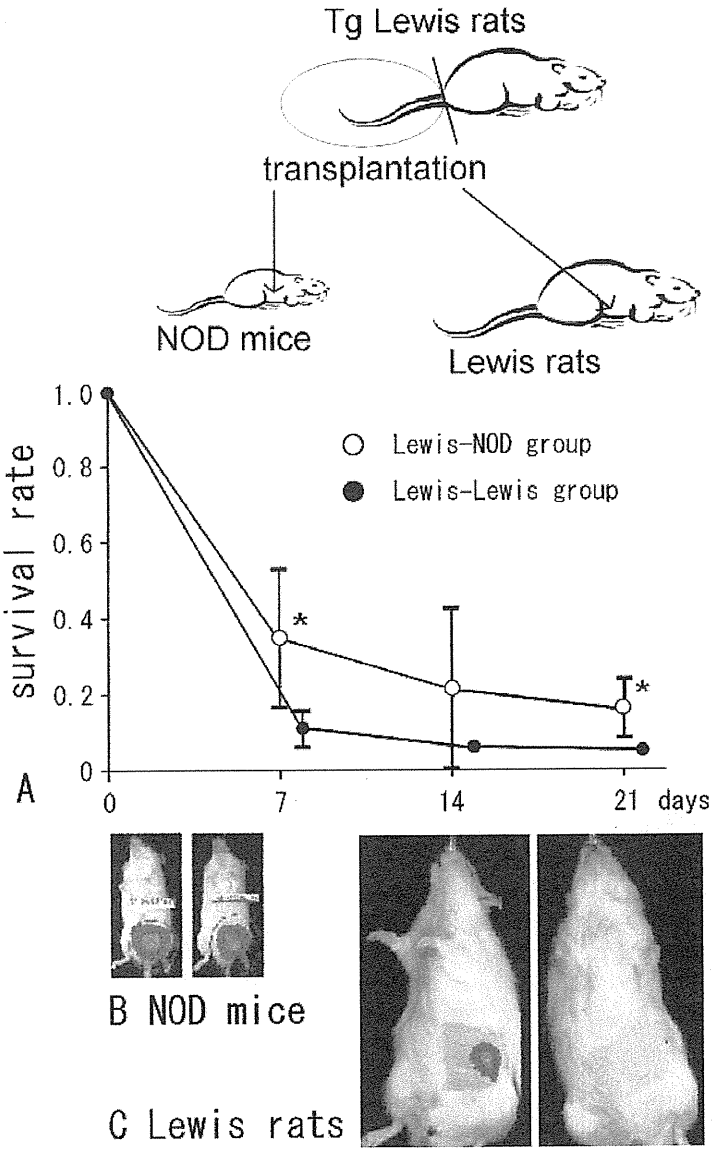

Fig. 3. (A) Survival rate of transplanted NP cells in Lewis rats and NOD mice (n=4, each). Closed circle indicates Lewis-Lewis group and open circle indicates Lewis-NOD group. Because intensity of luminescence is positively linear to the number of NP cells (data not shown), survival rate of NP cells was calculated as follows:

$$\text{Survival rate} = \frac{\text{Intensity of luminance after 7, 14 or 21 days}}{\text{Intensity of luminance just after transplantation}} \quad (2)$$

so that baseline value of survival rate (day 0) is "1". The survival rate was higher in the Lewis-NOD group than in the Lewis-Lewis group (*$p < 0.05$). (B) BLI imaging of NOD mouse at day 0 (left) and at day 90 (right). (C) BLI imaging of Lewis rat at day 0 (left) and at day 21 (right). NP cells hardly survived at day 21.

(Fig. 1B) and CFU-A (Fig. 1C) colonies revealed that larger numbers of spleen cells were attracted to CFU-NA colonies than to CFU-A colonies, further indicating that CFU-NA colony formation was more sensitive to the presence of spleen cells.

Cytotoxicity assay. From 10^8 Lewis rat spleen cells, $3.0x10^7$ CD4+T cells, $2.0x10^7$ CD8+T cells, $1.0x10^7$ macrophages and $6.0x10^6$ NK cells were sorted by FACS with data showing that more than 95% of the cells were alive.

Cytotoxicity to autologous NP cells was proportional to the E:T cell ratio in NK cells and macrophages (Fig. 2). At an E:T cell ratio of 100:1, cytotoxicity was 31-35% in NK cells and 9-20% in macrophages. Significant cytotoxicity was observed in NK cells at E:T cell ratios of 25:1 or more ($p < 0.0001$) and in macrophages at E:T cell ratios of 50:1 or more compared to the corresponding values in the absence of effector cells ($p = 0.001$ at 50:1; $p < 0.0001$ at 100:1) (Fig. 2). CD4+T cells and CD8+T cells did not have cytotoxic effects on NP cells.

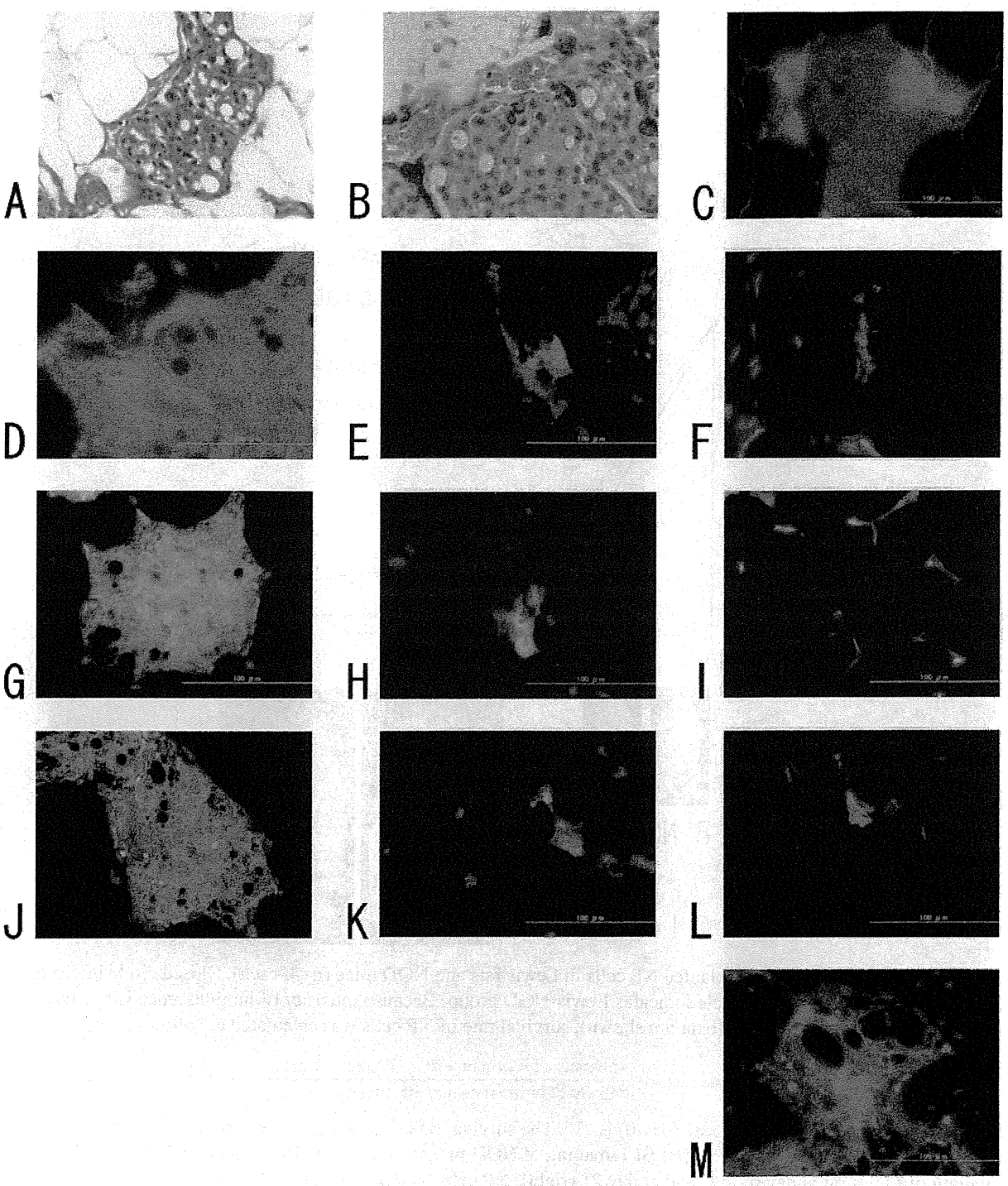

Fig. 4. Histological analysis of NPs at the transplant site of recipient rats. HE (A), safranin-O (B) and keratan sulphate IHC (C) staining indicate the presence of transplanted NPs at day 5. Safranin-O stains the proteoglycan of NPs (Red), and keratan sulphate is specific extracellular matrix of NPs (Green). Keratan sulphate was stained even 26 days after transplantation in the recipient of NOD mouse (M).

CD3 (D~F), CD68 (G~I) and CD161 (J~L) (Red) are immunohistochemically double-stained with keratin sulphate (Green). D, G, and J are the results at day 5; E, H, and K at day 10; F, I, and L at day 40. Keratan sulphate decreased dependent on time, NK cells and macrophages decreased simultaneously.

To summarize, the results of the *in vitro* CFI and cytotoxicity assays revealed the presence of a spleen cell population that had cytotoxic effects on autologous NP cells. This cytotoxic spleen cell population is composed of sub-populations of NK cells and macrophages. Furthermore, as a negative control of cytotoxicity assay, we used fibroblast-like cells of *annulus fibrosus* origin. The result was that the fibroblast-like cells was tolerant to isogeneous spleen cells, however *nucleus pulposus* cells was sensitive. This result raised our test hypothesis that NP is sensitive to specific immune cells.

***In vivo* study**

BLI study. We performed a BLI study to investigate immunological responses to transplanted NP tissues *in vivo*. The BLI evaluation showed a significantly higher survival rate for transplanted NP cells in the Lew-NOD group compared to that in the Lew-Lew group totally ($p = 0.036$), at day 7 (0.35±0.18 *vs.* 0.11±0.05; $p = 0.042$) and at day 21 (0.16±0.08 *vs.* 0.03±0.02; $p = 0.037$) (Fig. 3A). After 90 days, up to 13% of the transplanted NP cells had survived in the Lew-NOD group (Fig.3B). NP cells transplanted into Lewis rats (Lew-Lew) did not survive past 21 days, when luminescence at the NP cell transplant site had decreased to near background levels (Fig.3C).

IHC staining. Because our results showed that transplanted NP cell survival was reduced in association with an immunological reaction, we used immunological staining to identify which types of immune cells had infiltrated. Transplanted NP tissues in rats at day 5 existed mainly in the loose subcutaneous fat tissue as an agglomeration of cells with a bubble-like extracellular matrix (Fig. 4A). Safranin-O staining showed the presence of red-stained proteoglycans (Fig. 4B), and fluorescent green-stained keratan sulphate, both of which are constituents of the extracellular matrix of the NP (Fig. 4C). We observed transplanted NP tissues at day 5 (Fig. 4D, G, J), however, the amount of transplanted NP tissue was markedly decreased at day 10 in the Lewis rats, while NP tissue was obviously present in NOD mice recipients even at day 26 (Fig. 4M). From the IHC evaluation of immune cells in Lewis rats, no CD3 positive T cells attraction were observed subcutaneously from day 5 to day 40 (Fig. 4D, E, F). Attraction of NK cells and macrophages was observed at days 5 and 10 around the outgrown NP tissues (Fig. 4G, H, J, K); however, neither NP tissues nor immune cells were observed at day 40 (Fig. 4I, L). The numbers of NK cells and macrophages in microscope fields that included agglomerated NP cell clusters decreased with time (Table 2).

Discussion

The precise mechanism of immunological involvement in the pathology of disc herniation has not been defined. We performed two immunological assays, the CFI and the cytotoxicity assay, using co-cultured NP and immune cells. We also developed an *in vivo* subcutaneous transplantation model and measured the survival rate of transplanted NP cells using the BLI method. IHC at the transplant site of the recipient rats was used to identify the immune cells.

The suppression of NP cell colony formation was observed to be dependent on the effector:target (E:T) cell ratio. We found that non-adherent (CFU-NA) colonies were more strongly suppressed by immune cells than adherent (CFU-A) colonies. Because NP cells are known to be heterogeneous (Chelberg *et al.*, 1995), this difference in colony formation may reflect the different epitopes recognized by immune cells, or possible differences in the immune privilege function, like the presence or absence of Fas ligand. Based on these possibilities, about 20% of the NP cell population were alive even at E:T cell ratio of 100:1, which appears to differ immunologically from other NP cells. Of particular interest was the assessment of direct

Table 2 The number of immune cells in a microscope field (x40)

	Day 5	Day 10	Day 40
T cell	None	None	None
NK cell	2-5	1	None
Macrophage	4-7	1-3	None

This table indicates the number of representative agglomerated NP cell clusters in the tissue specimen of transplanted site in Lewis rats. NK and macrophage cells were observed in the transplanted site in the early phase, whereas T cells were not observed. In day 40, neither NP tissues nor immune cells were observed.

cytotoxic function of the immunological cell types. The results of the cytotoxicity assays of isolated T, NK, and macrophage cells demonstrated that only the NK and macrophage cells had cytotoxic activity on NP cells. The target molecules and their location on the NP cells remain undefined; further biological and immunological studies are necessary.

The results of the BLI study showed differences in the survival rate of NP cells in the transplanted NP tissues between the Lewis rat and NOD mouse recipients. NP cells are known to undergo apoptosis (Park *et al.*, 2001), and intervertebral disc cells are thought to be able to behave as competent phagocytes (Jones *et al.*, 2008). However, these results do not explain the different survival rates of NP cells in the current study. Because the survival rate of NP cells was higher in immunodeficient mice than in Lewis rats, immunological functions are implicated. NOD/shi-scid mice lack mature lymphocytes, and have macrophage dysfunction, a reduced level of NK cell activity and absence of circulating immune components compared to wild-type mice. These factors may account for the difference in NP cell survival rate between NOD mice and Lewis rats in our study.

We also detected the infiltration of specific immune cells into the NP transplant sites; these results definitively demonstrate the immunological activity of these cell types against NP tissues. Macrophages and NK cells, but not T cells, were detected, although the presence of T and B cells in isolated human herniated discs and in experimental porcine models has been previously reported (Geiss *et al.*, 2007). Our results suggest an early immunological response after normal NP tissues were exposed to the immune system. Thus, macrophages and NK cells were observed on days 5 and 10 when residual NP was present, but not on day 40 when the transplanted NP had disappeared. This finding supports the presence of an immunological response to transplanted NP tissues.

In our IHC study, CD68 positive cells did not resemble the appearance of resident chondrocytes. Although Jones *et al.* (2008) suggested that CD68 positive cells were transformed resident intervertebral disc cells, based on their morphology, the results of our study show that these macrophages are not transformed resident cells but rather are infiltrating cells.

Autologous tissues are generally not recognized as foreign by the immune system. The NP is an immune-privileged tissue isolated from the immune system (Hiyama *et al.*, 2008) and it, like similarly isolated tissues, including the eye and testis, can produce inflammatory autoimmune responses (Wildner and Diedrichs-Möhring, 2004; Schuppe and Meinhardt, 2005). Another possible trigger for autoimmunity is innate immunity, which is induced by chemical factors without specific antigen-antibody responses, leading to rapid immune responses to pathological microbe antigens. Because the NP cell produces chemical factors and the carbohydrate structure of the extracellular matrix produced by NP cells may mimic that of pathological microbe antigens, the NP may trigger an innate immunity response (Bárdos *et al.*, 2005).

In the *in vivo* transplantation model, we utilized a xenogeneic model because the mouse is too small to obtain enough donor NP cells. The use of NOD mice as recipients is well established for evaluating the effects of immunodeficiency. In addition, the xenogeneic transplantation model is commonly used for immunological evaluation (Yoshino *et al.*, 2000).

In conclusion, even non-degenerated NP cells elicit an immune response, and macrophages and NK cells in particular are shown to have an early immunological function when NP cells are exposed to the immune system. While these results may not be directly applicable to the human, this study provides important information for understanding the pathophysiological mechanism of disc herniation.

Acknowledgements

This work was supported in part by a Grant-in-Aid for Scientific Research and a Grant of The Science Frontier Program from the Ministry of Education, Culture, Sports, Science and Technology of Japan (D.S. and J.M.), grants from AO Spine International (D.S.), and Jichi Medical University.

References

Bárdos T, Szabó Z, Czipri M, Vermes C, Tunyogi-Csapó M Urban MR, Mikecz K, Glant TT (2005) A longitudinal study on an autoimmune murine model of ankylosing spondylitis. Ann Rheum Dis **64**: 981-987.

Bobechko WP, Hirsh C (1965) Auto-immune response to *nucleus pulposus* in the rabbit. J Bone Joint Surg Br **47**: 574-580.

Burke JG, Watson RWG, McCormack D, Dowling FE, Walsh MG, Fitzpatrick JM (2002) Spontaneous Production of Monocyte Chemoattractant Protein-1 and Interleukin-8 by the Human Lumbar Intervertebral Disc. Spine **27**: 1402-1407.

Chelberg MK, Banks GM, Geiger DF, Oegema TR Jr (1995) Identification of heterogeneous cell populations in normal human intervertebral disc. J Anat **186**: 43-53.

Doita M, Kanatani T, Ozaki T, Matsui N, Kurosaki M, Yoshiya S (2001) Influence of macrophage infiltration of herniated disc tissue on the production of matrix metalloproteinases leading to disc resorption. Spine **26**: 1522-1527.

Geiss A, Larsson K, Rydevik B, Takahashi I, Olmarker K (2007) Autoimmune Properties of *Nucleus Pulposus*: An Experimental Study in Pigs. Spine **32**: 168-173.

Geiss A, Larson K, Junevik K, Rydevik B, Olmarker K (2008) Autologous *nucleus pulposus* primes T cell to develop into interleukin-4-producing cells: an experimental study on the autoimmune properties of *nucleus pulposus*. J Orthop Res **27**: 97-103.

Gertzbein M, Tail M, Gross A, Falk R (1975) Autoimmunity in degenerative disc disease of the lumbar spine. Orthop Clin North Am **6**: 67-73.

Haro H, Craford HC, Fingleton B (2000) Matrix metalloproteinase-7–dependent release of tumor necrosis

factor-α in a model of herniated disc resorption. J Clin. Invest., **105**: 143-150.

Hiyama A, Mochida J, Iwashina T, Omi H, Watanabe T, Serigano K,Tamura F, Sakai D (2008) Transplantation of mesenchymal stem cells in a canine disc degeneration model. J Orthop Res **26**: 589-600.

Ikeda T, Nakamura T, Kikuchi T, Umeda S, Senda H, Takagi K (1996) Pathomechanism of spontaneous regression of the herniated lumbar disc: Histologic and immunohistochemical study. J Spinal Disord **9**: 136-140.

Jones P, Gardner L, Menaga J, Williams G, Roberts S (2008) Intervertebral disc cells as competent phagocytes *in vitro*: implications for cell death in disc degeneration. Arthritis Res Ther **10**: R86.

Kang JD, Georgescu HI, McIntyle-Larkin L, Stefanovic-Racic M, Donaldson WF 3rd, Evans CH (1996) Herniated lumbar intervertebral discs spontaneously produce matrix metalloproteinases, nitric oxide, interleukin-6, prostaglandin E2. Spine **21**: 271-277.

Katsuno R, Hasegawa T, Iwashina T, Sakai D, Mikawa Y, Mochida J (2008) Age-related effects of cocultured rat *nucleus pulposus* cells and macrophages on nitric oxide production and cytokine imbalance. Spine **33**: 845-849.

Le Maitre CL, Hoyland JA, Freemont AJ (2007) Catabolic cytokine expression in degenerate and herniated human intervertebral discs: IL-1**b** and TNF**a** expression profile. Arthritis Res Ther **9**: R77.

McCarron RF, Wimpee MW, Hudkins PG, Laros GS (1987) The inflammatory effect of *nucleus pulposus*. A possible element in the pathogenesis of low back pain. Spine **12**: 760-764.

Nachemson A (1969) Intradiscal measurements of pH in patients with lumbar rhizopathies. Acta Orthop Scand **40**: 23-42.

Park JB, Chang H, Kim KW (2001) Expression of Fas ligand and apoptosis of disc cells in herniated lumbar disc tissue. Spine **26**: 618-621.

Park JB, Chang H, Kim YS (2002) The pattern of interleukin-12 and T-helper types 1 and 2 cytokine expression in herniated lumbar disc tissue. Spine **27**: 2125-2128.

Satoh K, Konno S, Nishiyama K, Olmarker K, Kikuchi S (1999) Presence and distribution of antigen-antibody complexes in the herniated *nucleus pulposus*. Spine **24**: 1980-1984.

Schuppe HC, Meinhardt A (2005) Immune privilege and inflammation of the testis. Chem Immunol Allergy **88**: 1-14.

Spitzer G, Verma DS, Fisher R, Zander A, Vellekoop L, Litam J (1980) The myeloid progenitor cell – its value in predicting hematopoietic recovery after autologous bone marrow transplantation. Blood **55**: 317-323.

Virri J, Gronblad M, Seitsalo S, Habetemarian A, Kappa E, Karahaju E (2001) Comparison of the prevalence of inflammatory cells in subtypes of disc herniations and associations with straight leg raising. Spine **26**: 2311-2315.

Wang XM, Terasaki PI, Rankin GW Jr., Chia D, Zhong HP, Hardy S (1993) A new microcellular cytotoxicity test based on calcein AM release. Hum Immunol **37**: 264-270.

Weiler C, Nerlich BE, Boos N (2005) Expression and distribution of tumor necrosis factor alpha in human lumbar intervertebral discs: A study in surgical specimen and autopsy controls. Spine **30**: 44-53.

Wildner G, Diedrichs-Möhring M (2004) Autoimmune uveitis and antigenic mimicry of environmental antigens. Autoimmun Rev **3**: 383-387.

Yoshino H, Ueda T, Kawahata M, Kobayashi K, Ebihara Y, Manabe A, Tanaka R, Ito M, Asano S, Nakahata T, Tsuji K (2000) Natural killer cell depletion by anti-asialo GM1 antiserum treatment enhances human hematopoietic stem cell engraftment in NOD/Shi-scid mice. Bone Marrow Transplantation **26**: 1211-1216.

Development of the hyperspectral cellular imaging system to apply to regenerative medicine

Miya Ishihara*[a], Masato Sato [b], Kouji Matsumura [c], Joji Mochida [b], Makoto Kikuchi [a]
[a] Dept. of Medical Engineering, National Defense Medical College,
3-2 Namiki, Tokorozawa, Saitama Japan 359-8513
[b] Dept. of Orthopaedic Surgery, Tokai University School of Medicine
143 Shimokasuya, Isehara, Kanagawa Japan 259-1193
[c] Central Research Laboratory, National Defense Medical College,
3-2 Namiki, Tokorozawa, Saitama Japan 359-8513

ABSTRACT

Regenerative medicine by the transplantation of differentiated cells or tissue stem cells has been clinically performed, particularly in the form of cell sheets. To ensure the safety and effectiveness of cell therapy, the efficient selection of desired cells with high quality is a critical issue, which requires the development of a new evaluation method to discriminate cells non-invasively with high throughput. There were many ways to characterize cells and their components, among which the optical spectral analysis has a powerful potential for this purpose. We developed a cellular hyperspectral imaging system, which captured both spatial and spectral information in a single pixel. Hyperspectral data are composed of continual spectral bands, whereas multispectral data are usually composed of about 5 to 10 discrete bands of large bandwidths. The hyperspectral imaging system which we developed was set up by a commonly-used inverted light microscope for cell culture experiments, and the time-lapse imaging system with automatic focus correction. Spectral line imaging device with EMCCD was employed for spectral imaging. The system finally enabled to acquire 5 dimensional (x, y, z, time, wavelength) data sets and cell-by-cell evaluation. In this study, we optimized the protocol for the creation of cellular spectral database under biological understanding. We enabled to confirm spectrum of autofluorescence of collagen, absorption of specific molecules in the cultural sample and increase of scattering signal due to cell components although detail spectral analyses have not been performed.

Keywords: hyperspectral imaging, cellular function, intrinsic optical spectrum, regenerative medicine, cell sheet,

1. INTRODUCTION

Regenerative medicine is now developed to a practical level. The transplantation of differentiated cells or tissue stem cells has been clinically performed, particularly in the form of cell sheets and also engineered tissue. To ensure the safety and effectiveness of cell therapy and sheet transplantation, the efficient selection of desired cells with high quality is a critical issue, which requires the development of a new evaluation method to discriminate cells non-invasively. The required evaluation method should enable to discriminate cells in culture condition of monolayer or cell-sheet. There were many ways to characterize cells and their components, among which the intrinsic optical spectral analysis has a powerful potential for this purpose [1].

*kobako@ndmc.ac.jp, phone +81-4-2995-1211

Optics in Tissue Engineering and Regenerative Medicine IV, edited by Sean J. Kirkpatrick, Ruikang Wang,
Proc. of SPIE Vol. 7566, 756606 · © 2010 SPIE · CCC code: 1605-7422/10/$18 · doi: 10.1117/12.841758

There are several possible situations to discriminate cells using intrinsic optical spectra [2]. Cell cycle is one of key factors for the cell characterization. Different Cell phase, such as cell in S-phase and in M-phase has completely different cellular character. Chromatin is contributing factor in genomic change and cell cycle modulation. The microscopic observation of chromatin would be easily accepted as highly scattering substance in the nuclear. The scattering parameter of chromatin would be extracted depending on the cell cycle. Collagen, as major contents of extracellular matrix, is autofluorescence substance. The formation of pericellular matrix would be monitored, which directly related cell-sheets' function. Mitochondria would denote energy status of cell and relating NADH complex, which is well-known optical absorber. Therefore, quantitative optical parameters are potentially very helpful in determining the cellular character.

Our ultimate goal is to develop a total cellular imaging system demonstrating useful intracellular and/or extracellular spectrum including proper analyses, which enables to discriminate desired cells for cell safety and efficacy for application to regenerative medicine. That is, the intrinsic optical spectrum, which has a relation to cellular biological understanding, could indicate whether the cell can be practically applied to regenerative medicine.

2. BUILD UP HYPERSPECTRAL CELLULAR IMAGING SYSTEM

2.1 Hyperspectral Imaging

Hyperspectral imaging devices are common in remote sensing reconnaissance. It captures both spatial and spectral information in a single pixel. Hyperspectral imaging collects the same picture at different wavelength to generate a "datacube" that can reveal objects. Another advantage of this imaging form is that different element leaves unique spectral signatures behind in various bands of the spectrum. Using these specific signatures, it is possible to identify the materials that make up an observed object.

We developed microscopic hyperspectral imaging system in order to discriminate cells and demonstrated the optimal protocol to obtain the spectrum of arbitrary intracellular and/or extracellular region. The system was equipped with time-lapse microscopy and spectroscopic imaging apparatus including an EMCCD detector described details below (2.2 – 2.4). The protocol for spectral acquisition was determined for synchronizing the hyperspectral image with general microscopic image.

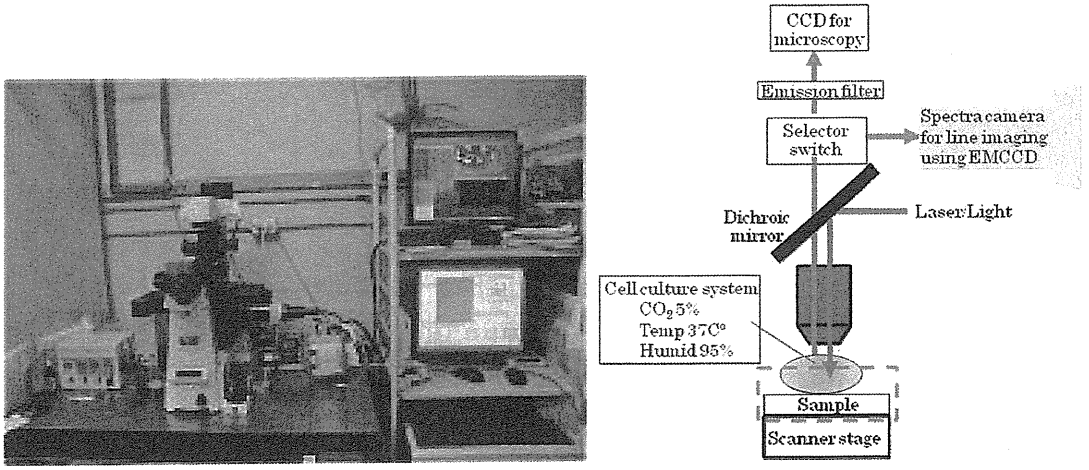

Fig.1 Apparatus for the hyperspectral cellular imaging system (The system configuration in the photograph (left) refers to the drawing (right))

2.2 Components - 1. Time-lapse microscopy

Integrated flexible microscope system (Nikon, ECLIPSE Ti) which allowed high-speed screening image capture was employed. The microscope system has faster operation speed which could reduce overall light exposure. It was equipped with time-lapse imaging with automatic focus correction system and CO_2 incubator cell culture system. The time-lapse image enabled that the same object (e.g., a cell) is photographed at regular time intervals over several hours. The time-lapse serial data allow us to observe the morphological change in the process of differentiation and/or lineage conversion such as iPSC emergence which could be definitively confirmed by its shape [3].

2.3 Components - 2. Imaging spectrograph

ImSpector V8 (Specim) was employed as the imaging spectrograph in our system. It has visible range (380-800 nm) with 8 nm spectral resolution. It works as a spectral line imaging device which produces full contiguous spectral information in each line pixel with high spectral resolution to provide a push-broom hyperspectral operation.

2.4 Components - 3. EMCCD and Software

Andor's iXon^{EM}+DU-897 back illuminated EMCCD (Electron Multiplying Charge Coupled Device) was employed. Its active pixels were 512 x 512 and frame rate is 35 fps. The 'on-chip' amplification process of the EMCCD was realized without sacrificing the photon collection capability of the sensor, with back-illuminated sensors offering up to 95% Quantum Efficiency (QE). Thus, the system was equipped with a suitable sensor. Original software for the hyperspectral operation was developed linked to general microscopic image. The line scanned hyperspectral image were confirmed as identical system to the general microscopic image precisely.

Table 1 Feature of the developed system

Wavelength range	380~780nm
Spectroscopic tool	Spectral line imaging
Spectral resolution	8nm
Image resolution	X axis : 30μm/object lens magnification
	Y axis : microscopic view field/512 pixels
Imaging rate	35 frame/sec maximum
Noise reduction	Dark-current and thermal noise correction
Image processing Image display	-Color image display from spectrum to RGB conversion
	-Spectral display at each pixel
	-Image display at specific wavelength
	-Calculation function of color difference

3. PROTOCOL FOR DETERMININATION OF INDIVIDUAL SPECTRUM OF ARBITRARY INTRACELLULAR AND/OR EXTRACELLULAR REGIONS

The cell-related known spectra to date might not be proven because the spectra were obtained under undefined biological aspect. The spectra of cell components (nuclear chromatin, subcellular organelle and extracellular matrix) for regenerative medicine should be determined under biological realistic condition. Consequently, in order to reach our ultimate goal, spectral database should be created on biological understanding at the first step in order to ensure cell safety and effectiveness using the intrinsic spectrum of arbitrary intracellular and/or extracellular region. That is, proper protocol for the spectral acquisition should be designed. In this study, light source has not been optimized yet.